Topological instabilities in ac-driven bosonic systems

Georg Engelhardt, Mónica Benito, Gloria Platero, Tobias Brandes

Angaben zur Veröffentlichung / Publication details:

Engelhardt, Georg, Mónica Benito, Gloria Platero, and Tobias Brandes. 2016. "Topological instabilities in ac-driven bosonic systems." *Physical Review Letters* 117: 045302. https://doi.org/10.1103/PhysRevLett.117.045302.

Topological Instabilities in ac-Driven Bosonic Systems

G. Engelhardt,[1,*] M. Benito,[2] G. Platero,[2] and T. Brandes[1]
[1]Institut für Theoretische Physik, Technische Universität Berlin, Hardenbergstrasse 36, 10623 Berlin, Germany
[2]Instituto de Ciencia de Materials de Madrid, CSIC, 28049 Madrid, Spain
(Received 4 January 2016; published 21 July 2016)

Under nonequilibrium conditions, bosonic modes can become dynamically unstable with an exponentially growing occupation. On the other hand, topological band structures give rise to symmetry protected midgap states. In this Letter, we investigate the interplay of instability and topology. Thereby, we establish a general relation between topology and instability under ac driving. We apply our findings to create dynamical instabilities which are strongly localized at the boundaries of a finite-size system. As these localized instabilities are protected by symmetry, they can be considered as topological instabilities.

DOI: 10.1103/PhysRevLett.117.045302

Introduction.—Because of their underlying symplectic structure, bosonic systems can exhibit so-called dynamical instabilities [1–3]. This effect can occur in the presence of nonparticle conserving terms which appear, e.g., in the Bogoliubov excitations of Bose-Einstein condensates. Thereby, the bosonic occupation of a mode grows exponentially in time due to a nonequilibrium state of the system. On the other hand, the theory of topological band structures predicts symmetry protected midgap states [4–13]. *A priori*, dynamical instability and topology are independent phenomena.

In this Letter, we formalize a relation between instabilities and topology under ac driving. More precisely, we explain that different topological phases are separated by regions of instability. Using this relation, we demonstrate how to employ topology to systematically engineer topologically protected dynamical instabilities. Thereby, spatially localized midgap modes are rendered dynamically unstable with exponentially growing bosonic occupation as has been exemplarily proposed for Bose-Einstein condensates in Refs. [11,14,15], and for photonic systems [16]. Here, we suggest a very flexible tool in the form of ac fields in order to engineer topological instabilities governed by corresponding artificial, effective Hamiltonians [17]. This simultaneously provides us the possibility to detect the midgap states as their occupation increases exponentially in time. Topological instabilities are an effect with no direct analogue in fermionic topological insulators. This stresses the need for a more intensive investigation of topological effects in bosonic systems.

In fermionic systems, ac driving has been applied to control topological phases [18–24]. In particular, the topology of a band can change if there is a degeneracy of the form $\epsilon_{i'} = \epsilon_i + \Omega$, where Ω denotes the driving frequency. As this is a single-particle effect, it can also appear in bosonic systems [25,26]. The main challenge, however, is that dynamical instabilities appearing in bosonic systems generated by an ac field constitute an obstruction in the search for a stable system with nontrivial topology [25]: by slightly changing parameters, the system might get unintentionally unstable within the bulk, which obscures the existence of midgap states. For the one-dimensional Hamiltonian under consideration, we show how to employ stability diagrams to facilitate the search of adequate system parameters. The latter can be regarded as a higher-dimensional version of the famous Arnold tongues in parametrically driven oscillators [3].

Selective enhancement of edge states and related effects can be achieved using different approaches, e.g., non-Hermitian Hamiltonians [27–30]. Furthermore, in a driven spin chain the crossing of topological phase transitions is accompanied by a Kibble-Zurek scaling phenomenon [31]. These effects raise the question, to what extent the instability-topology relation established here for bosonic ac-driven systems can be generalized to other fields of physics.

The system.—Bogoliubov Hamiltonians are important in many areas of physics. For instance, they appear when expanding Hamiltonians describing interacting bosonic particle or polariton condensates in orders of the fluctuations [1,2,14,32]. They also describe excitations in magnonic crystals [8,9] or in quantum-optical systems [33]. More generally, they appear in the linear stability analysis of nonlinear bosonic systems [34].

We analyze a one-dimensional system of coupled bosonic modes which is subjected to periodic driving. However, we emphasize that the relation between instability and topology established here applies also for higher-dimensional systems. A Hamiltonian allowing for a systematic investigation of the topological instabilities which we are interested in reads

$$H = \sum_m -(\nu(t)\hat{a}^\dagger_{m,1}\hat{a}_{m,2} + \nu'(t)\hat{a}^\dagger_{m,2}\hat{a}_{m+1,1} + \text{H.c.}) + g\sum_{m,s=\{1,2\}}(\hat{a}^\dagger_{m,s}\hat{a}^\dagger_{m,s} + \text{H.c.}) - \sum_{m,s=\{1,2\}}\mu\hat{a}^\dagger_{m,s}\hat{a}_{m,s}, \quad (1)$$

where $\hat{a}_{m,s}$ with $s = 1, 2$ are bosonic annihilation operators, $\nu(t) \equiv \nu_0 + \nu_1 \cos(\Omega t)$, $\nu'(t) \equiv \nu'_0 + \nu'_1 \cos(\Omega t)$ and μ is the chemical potential. The system is sketched in Fig. 1(a). For $\nu_1 = \nu'_1 = 0$ the first line resembles the famous Su-Schrieffer-Heeger model which exhibits a topological phase transition for $\nu_0 = \nu'_0$ [35]. Because of the non-particle-conserving terms in the second line the bosonic modes can exhibit dynamical instabilities with exponentially growing bosonic occupation.

After a transformation into the momentum space, the Bogoliubov Hamiltonian reads

$$\hat{H}^{(B)}(t) = \frac{1}{2}\sum_k (\hat{\mathbf{a}}_k^\dagger, \hat{\mathbf{a}}_{-k}) \mathbf{H}_k(t) \begin{pmatrix} \hat{\mathbf{a}}_k \\ \hat{\mathbf{a}}_{-k}^\dagger \end{pmatrix}. \tag{2}$$

The symbol $\hat{\mathbf{a}}_k^\dagger = (\hat{a}_{k,1}^\dagger, \hat{a}_{k,2}^\dagger)$ denotes a vector of bosonic creation operators, and

$$\mathbf{H}_k(t) \equiv \mathbb{1} \otimes \vec{h}(k,t)\vec{\sigma} - \mu \mathbb{1} \otimes \mathbb{1} + g\sigma_x \otimes \mathbb{1}, \tag{3}$$

where $\vec{\sigma} = (\sigma_x, \sigma_y)$ is a vector of Pauli matrices and we defined a pseudo magnetic-field vector with components $h_x(k,t) = -\nu(t) - \nu'(t)\cos k \equiv h_{x,0}(k) + h_{x,1}(k)\cos\Omega t$ and $h_y(k,t) = -\nu'(t)\sin k \equiv h_{y,0}(k) + h_{y,1}(k)\cos\Omega t$.

Importantly, the Bogoliubov Hamiltonian fulfills a generalized chiral symmetry at all times t. This is defined by

$$\begin{aligned} &\Sigma[\mathbf{H}_k(t) + \mu\mathbb{1} \otimes \mathbb{1} - g\sigma_x \otimes \mathbb{1}]\Sigma \\ &\quad = -[\mathbf{H}_k(t) + \mu\mathbb{1} \otimes \mathbb{1} - g\sigma_x \otimes \mathbb{1}], \end{aligned} \tag{4}$$

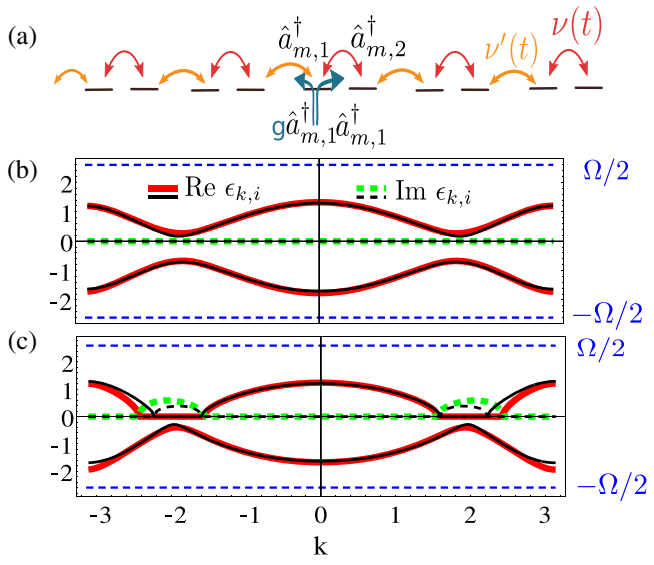

FIG. 1. (a) Sketch of the system. (b) and (c) depict quasienergy spectra with colored lines for $\nu_0 = 1.5$, $\nu'_0 = 0$, $\nu_1 = 3$, $\mu = -5$ and $\Omega = 5.2$. We choose $\nu'_1 = 11$ and $\nu'_1 = 6$ in (b) and (c), respectively. Black lines depict the spectrum of an effective Hamiltonian [36]. All quantities are expressed in units of g.

where $\Sigma = \sigma_z \otimes \sigma_z$. Accordingly, the Hamiltonian corresponds to the topological class BDI according to the Altland-Zirnbauer classification [37]. The band structure of the undriven and noninteracting system exhibits two bands. They are described by a topological quantum number given by

$$W = \frac{1}{2\pi i}\int_{-\pi}^{\pi} \frac{d}{dk} \ln\left[h_x(k) + ih_y(k)\right], \tag{5}$$

which counts how often the vector $\vec{h}(k)$ winds around $\vec{h}(k) = 0$. Consequently, W can only change if there is a degeneracy, as this is related to $\vec{h}(k) = 0$. By definition, the winding number describes translational invariant systems. However, there is an important consequence for finite-sized systems with boundaries. There are spatially confined states close to the boundary with energy located within the band gap. The number of these states equals W [6,38]. We now show how the physics is modified in the presence of periodic driving and interactions.

Floquet-Bogoliubov theory.—As regular Bogoliubov excitation energies of an undriven system, the Floquet-Bogoliubov quasienergies for bosons reveal the stability of a system. It is stable, if all quasienergies are real-valued and unstable if one or more have a finite imaginary part. They can be obtained as follows [1–3,25,39,40]: first, we have to solve the differential equation

$$i\frac{d}{dt}\mathbf{U}(t) = \boldsymbol{\sigma}_z \mathbf{H}(t)\mathbf{U}(t), \qquad \mathbf{U}(0) = \mathbf{1}, \tag{6}$$

where $\boldsymbol{\sigma}_z = \sigma_z \otimes \mathbb{1}$ emerges as the Bogoliubov Hamiltonian couples bosonic creation and annihilation operators, whose equations of motion differ by a minus sign. The matrix $\mathbf{U}(2\pi/\Omega)$ is the Floquet operator and its eigenvalues and eigenstates fulfill

$$\mathbf{U}(2\pi/\Omega)|\Psi_i\rangle = e^{-i(2\pi/\Omega)\epsilon_i}|\Psi_i\rangle, \tag{7}$$

where ϵ_i denotes the Bogoliubov quasienergies and $|\Psi_i\rangle$ the stroboscopic Floquet states [34]. There are always $2d$ Floquet states where d denotes the dimension of the single-particle Hamiltonian. As usual quasienergies, the real part of the Bogoliubov quasienergies can be represented within the window $(-\Omega/2, \Omega/2)$. A system is only stable if the quasienergies for all $k \in (-\pi, \pi)$ are real valued. In this case we denote the system to be globally stable.

Additionally, we introduce the concept of strong stability according to Refs. [3,40]. A Floquet state with Im $\epsilon_i = 0$ is denoted to be *strongly* stable, if a small perturbation of the system does not result in a finite imaginary part Im $\epsilon_i \neq 0$. If a state is strongly stable, then it can be normalized as $C_i \equiv \langle\Psi_i|\boldsymbol{\sigma}_z|\Psi_i\rangle = \pm 1$ [1,40]. For every state with ϵ_i there is a corresponding state with $\epsilon_{i'} = -\epsilon_i$. If the states are

normalizable, then $C_i = -C_{i'}$. A system is considered to be strongly stable, if all Floquet states are strongly stable.

Two Bogoliubov quasienergy dispersions are depicted in Figs. 1(b) and 1(c), where we take the state with $C_{k,i} = 1$ if it is normalizable. In panel (c), we recognize momenta k with $\mathrm{Im}\,\epsilon_{k,i} \neq 0$, leading to a dynamical instability with bosonic occupations growing exponentially in time [1,2], which we analyze in Fig. 2(a), where the system is not globally stable in the green areas.

Following Refs. [3,40], one finds that if the quasienergies of two strongly stable states with $C_i \neq C_j$ merge by varying system parameters, thus, they become

$$\mathrm{Re}\,\epsilon_i = \mathrm{Re}\,\epsilon_j \bmod \Omega, \tag{8}$$

then the states are not strongly stable. Moreover, even when becoming unstable, the states i, j still fulfill Eq. (8) which thus constitutes a necessary instability condition. Consequently, if the quasienergy of an originally strongly stable state gets $\mathrm{Re}\,\epsilon_i = 0, \Omega/2$, it is not strongly stable. We relate this to topology in the following.

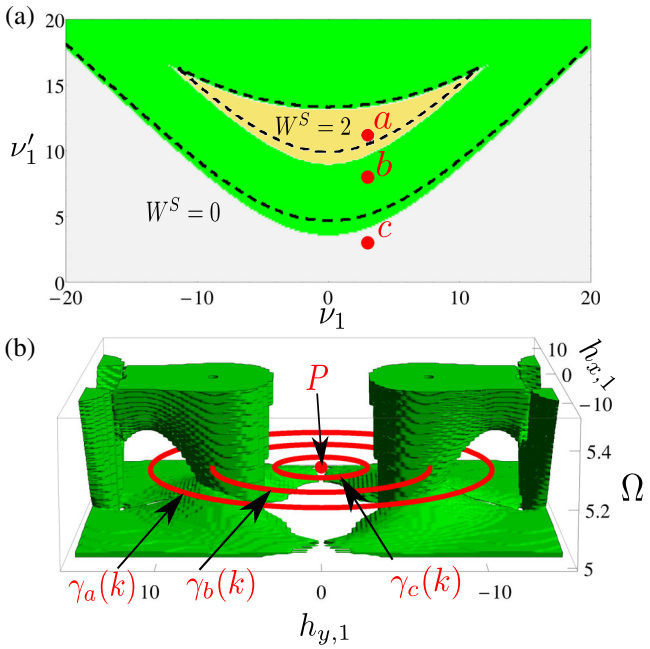

FIG. 2. (a) Topological phase diagram. The parameters are as in Fig. 1(b). In the green (dark gray) areas, the system is not globally stable, so the topological invariant W^S in Eq. (9) is not defined there. In the white and yellow (light gray) areas, we find that $W^S = 0$ and $W^S = 2$, respectively. The topological phases are separated by instability areas (green). Dashed lines are obtained by using an effective Hamiltonian [36]. (b) Stability diagram as a function of $h_{x,1}$ and $h_{y,1}$ corresponding to (a). The parameters of the curves $\gamma_{a,b,c}$ are depicted in (a) by the points $p = a, b, c$. The parameters $p = a$ and $p = b$ correspond to Figs. 1(b) and 1(c). Curve γ_c can be contracted to point P, so that it is topologically trivial according to the explanations in the main text.

Topology.—Motivated by Refs. [8,10], we define a topological invariant generalizing Eq. (5) for driven bosonic Bogoliubov systems by

$$W^S \equiv \frac{1}{\pi i}\sum_{i\in\mathcal{S}}\int_{-\pi}^{\pi} dk \langle\Psi_{k,i}|\boldsymbol{\sigma}_z \frac{d}{dk}|\Psi_{k,i}\rangle, \tag{9}$$

where $\mathcal{S} = \{i | 0 < \epsilon_{k,i} < \Omega/2 \wedge C_{k,i} = 1 \text{ for all } k\}$ is the set of all positive normalizable quasienergies. We note that W^S is only defined for globally strongly stable systems.

As our Hamiltonian fulfills a generalized chiral symmetry, the topological invariant is integer valued, i.e., $W^S \in \mathbb{Z}$. It predicts midgap states energetically located close to $\epsilon_i = 0, \Omega/2$, thus, close to the instability condition, Eq. (8). The number of midgap states at each boundary equals W^S.

The topological phase diagram is depicted in Fig. 2(a). There we find a phase with $W^S = 0$ (white) and one with $W^S = 2$ (yellow). Interestingly, these two phases are separated by instability regions which is a general feature in driven bosonic systems, cf. below.

Instability-topology relation.—We are now in a position to establish a general relation between topology and instability of a bosonic system under ac driving: The topological invariant, Eq. (9), can only change by a smooth variation of system parameters $p(t)$ with $t \in [0, 1]$, if the system is not globally strongly stable for at least one $t = t_0$.

The relation is a direct consequence of the instability condition Eq. (8). When we only perform parameter variations so that the system is globally strongly stable, Eq. (8) is never fulfilled and $\mathcal{S}$ remains unchanged. Moreover, the bands $i \in \mathcal{S}$ are not in contact with the bands $i \neq \mathcal{S}$ so that the topological invariant cannot change.

By definition, in the vicinity of stable but not strongly stable parameters there are always unstable parameters. Consequently, the topological phases in Fig. 2(a) are separated by unstable regions.

We emphasize that this relation is valid for systems of arbitrary dimensions. One only has to replace W^S in Eq. (9) by a higher-dimensional topological invariant.

To elucidate this relation, we investigate the stability of the Hamiltonian [Eq. (2)] as a function of $h_{\eta,1}$ with $\eta = x, y$ and Ω. The result is depicted in Fig. 2(b), where we depict unstable parameters in green. A set of system parameters p specifies a curve as a function of momentum k in the stability diagram due to the parametrization of $h_{\eta,1}$ with $\eta = x, y$ below Eq. (3). For instance, the points $p = a, b, c$ depicted in Fig. 2(a) correspond to curves $\gamma_p(k)$ in the stability diagram in Fig. 2(b). The curves γ_a and γ_c do not traverse any unstable areas, so they are globally stable, while γ_b is not.

If one can smoothly contract a globally strongly stable $\gamma(k)$ while clearly avoiding areas of unstable parameters, then $W^S_\gamma = 0$. In Fig. 2(b), $\gamma_c(k)$ can be trivially contracted to P so that it has a trivial topology. By contrast, the

deformation of $\gamma_a(k)$ onto a stable point in Fig. 2(b), is only possible by traversing the two unstable green regions. For this reason, it is a candidate for a nontrivial topology with $W_\gamma^S \neq 0$. We thus have a one-to-one correspondence between *points* in the topological phase diagram in Fig. 2(a), and (non-) contractible *curves* in the stability diagram in Fig. 2(b).

Moreover, the stability diagram assists in finding parameters corresponding to a stable and topological-nontrivial system. We only have to calculate W^S for noncontractible curves which cannot be transformed to each other in a stable way.

The black lines in Figs. 1(b), 1(c) and 2(a) depict the calculations using a time-independent effective Hamiltonian [36]. For its derivation, we generalized the procedure of Ref. [23] to Bogoliubov Hamiltonians which, to our knowledge, has not been done before. As the effective Hamiltonian resembles the features of the spectrum, it is an appropriate tool to calculate stability diagrams which enable an efficient search for parameters of stable and topologically nontrivial systems.

Topological instabilities.—Because of its definition, W^S predicts midgap states energetically located close to $\epsilon_i = 0$, $\Omega/2$, thus, close to the instability condition [Eq. (8)]. In Fig. 3(a), we depict the numerical quasienergy spectrum for a finite-sized system with boundaries with parameters given by $p = a$ in Fig. 2(a). There are four midgap states with Re $\epsilon_i \approx 0$ which we mark with arrows. Their wave functions are strongly confined to the boundaries. The wave function of one of them is depicted in the inset of panel (b). The imaginary part of the quasienergies of two midgap states is finite, so they are dynamically unstable, which gives rise to an exponential growth of the occupation as a function of time. The imaginary part of the quasienergies of the other two midgap states is zero, so they are stable. The states not marked by an arrow are bulk modes and are stable.

In principle, one can render all four midgap states to be unstable by slightly adjusting the system parameters as Re $\epsilon_i \approx 0$. However, we did not find parameters where all four midgap states are unstable without destabilizing the bulk modes.

The initial state of the time evolution in Fig. 3(b) is the vacuum state defined by $\hat{a}_j|\text{vac}\rangle = 0$ [11,14,15]. We recognize, that the occupation grows exponentially on sites close to the boundary, while it remains small within the bulk. As the instabilities are generated by the unstable midgap states, they can be thus considered to be topologically protected instabilities.

To conclude, we found that topological phases are separated by regions of instability in ac-driven systems which we illustrated using stability diagrams. We recall that this finding is valid for systems of arbitrary dimension. We used this to selectively generate dynamical instabilities which are strongly localized close to the boundaries.

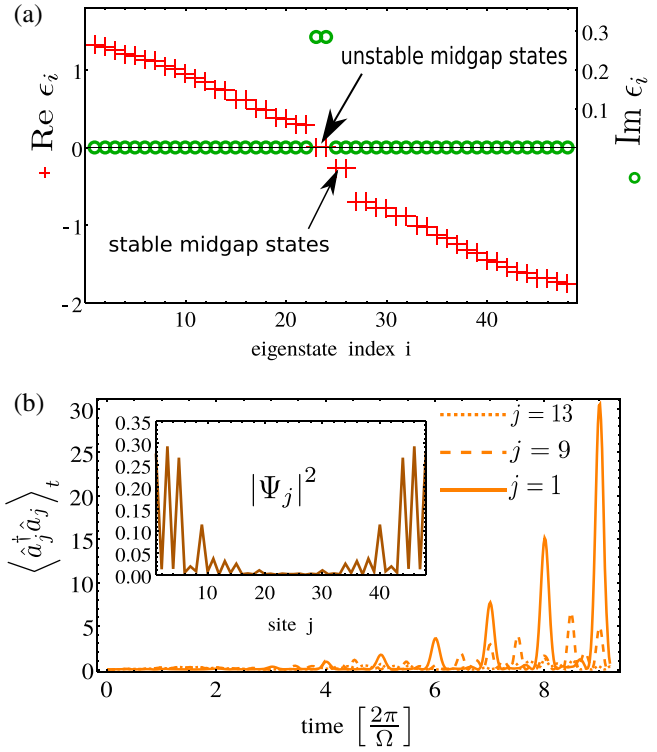

FIG. 3. (a) Quasienergy spectrum for a finite-sized system with boundaries corresponding to γ_a. There are four midgap states located near Re $\epsilon_i = 0$ which we mark with arrows. The imaginary part of two of the midgap states is finite, which renders these states unstable. States not marked by the arrows extend within the bulk and are stable. (b) Time evolution of the occupation of the sites $j = 1, 9, 13$. The initial state is the vacuum state. In the inset we depict the wave function $\Psi_j = \langle \text{vac}|\hat{a}_j|\Psi_i\rangle$ of one of the unstable midgap states which are responsible for the exponential growth as seen in (b). It is strongly confined close to the boundaries. Note that the site number is $j = 2m + s$, with m, s defined in Eq. (1).

To this end, we employed localized midgap states whose occupation grows exponentially in time. Recently, stability and the onset of chaos have been experimentally explored in a periodically driven two-mode Bose-Einstein condensate [41]. We assume that the spatially extended system investigated here is also a candidate for such an experimental investigation.

The authors gratefully acknowledge financial support from the DFG Grants No. BR 1528/7, No. BR 1528/8, No. BR 1528/9, No. SFB 910, and No. GRK 1558. This work was supported by the Spanish Ministry through Grant No. MAT2014-58241-P.

*georg@itp.tu-berlin.de

[1] Y. Kawaguchi and M. Ueda, Phys. Rep. **520**, 253 (2012).
[2] L. Goren, E. Mariani, and A. Stern, Phys. Rev. A **75**, 063612 (2007).

[3] V. I. Arnold, *Mathematical Methods of Classical Mechanics* (Springer Science & Business Media, New York, 1989), Vol. 60.
[4] B. A. Bernevig and T. L. Hughes, *Topological Insulators and Topological Superconductors* (Princeton University Press, Princeton, NJ, 2013).
[5] L. Fu and C. L. Kane, Phys. Rev. B **74**, 195312 (2006).
[6] M. Z. Hasan and C. L. Kane, Rev. Mod. Phys. **82**, 3045 (2010).
[7] G. Jotzu, M. Messer, R. Desbuquois, M. Lebrat, T. Uehlinger, D. Greif, and T. Esslinger, Nature (London) **515**, 237 (2014).
[8] R. Shindou, R. Matsumoto, S. Murakami, and J.-I. Ohe, Phys. Rev. B **87**, 174427 (2013).
[9] R. Shindou, J.-I. Ohe, R. Matsumoto, S. Murakami, and E. Saitoh, Phys. Rev. B **87**, 174402 (2013).
[10] G. Engelhardt and T. Brandes, Phys. Rev. A **91**, 053621 (2015).
[11] S. Furukawa and M. Ueda, New J. Phys. **17**, 115014 (2015).
[12] C.-E. Bardyn, T. Karzig, G. Refael, and T. C. H. Liew, Phys. Rev. B **93**, 020502 (2016).
[13] V. Peano, M. Houde, C. Brendel, F. Marquardt, and A. A. Clerk, Nat. Commun. **7**, 10779 (2016).
[14] R. Barnett, Phys. Rev. A **88**, 063631 (2013).
[15] B. Galilo, D. K. K. Lee, and R. Barnett, Phys. Rev. Lett. **115**, 245302 (2015).
[16] V. Peano, M. Houde, F. Marquardt, and A. A. Clerk, arXiv:1604.04179.
[17] V. M. Bastidas, C. Emary, B. Regler, and T. Brandes, Phys. Rev. Lett. **108**, 043003 (2012).
[18] M. C. Rechtsman, J. M. Zeuner, Y. Plotnik, Y. Lumer, D. Podolsky, F. Dreisow, S. Nolte, M. Segev, and A. Szameit, Nature (London) **496**, 196 (2013).
[19] Y. H. Wang, H. Steinberg, P. Jarillo-Herrero, and N. Gedik, Science **342**, 453 (2013).
[20] T. Oka and H. Aoki, Phys. Rev. B **79**, 081406 (2009).
[21] A. Kundu and B. Seradjeh, Phys. Rev. Lett. **111**, 136402 (2013).
[22] P. Wang, Q.-f. Sun, and X. C. Xie, Phys. Rev. B **90**, 155407 (2014).
[23] M. Benito, A. Gómez-León, V. M. Bastidas, T. Brandes, and G. Platero, Phys. Rev. B **90**, 205127 (2014).
[24] T. Mikami, S. Kitamura, K. Yasuda, N. Tsuji, T. Oka, and H. Aoki, Phys. Rev. B **93**, 144307 (2016).
[25] G. Salerno, T. Ozawa, H. M. Price, and I. Carusotto, Phys. Rev. B **93**, 085105 (2016).
[26] R. Fleury, A. Khanikaev, and A. Alu, arXiv:1511.08427.
[27] S. Malzard, C. Poli, and H. Schomerus, Phys. Rev. Lett. **115**, 200402 (2015).
[28] H. Schomerus, Opt. Lett. **38**, 1912 (2013).
[29] C. Poli, M. Bellec, U. Kuhl, F. Mortessagne, and H. Schomerus, Nat. Commun. **6**, 6710 (2015).
[30] J. M. Zeuner, M. C. Rechtsman, Y. Plotnik, Y. Lumer, S. Nolte, M. S. Rudner, M. Segev, and A. Szameit, Phys. Rev. Lett. **115**, 040402 (2015).
[31] A. Russomanno and E. G. Dalla Torre, arXiv:1510.08866.
[32] R. Bücker, J. Grond, S. Manz, T. Berrada, T. Betz, C. Koller, U. Hohenester, T. Schumm, A. Perrin, and J. Schmiedmayer, Nat. Phys. **7**, 608 (2011).
[33] C. Emary and T. Brandes, Phys. Rev. Lett. **90**, 044101 (2003).
[34] A. R. Kolovsky, H. J. Korsch, and E.-M. Graefe, Phys. Rev. A **80**, 023617 (2009).
[35] A. J. Heeger, S. Kivelson, J. R. Schrieffer, and W. P. Su, Rev. Mod. Phys. **60**, 781 (1988).
[36] See Supplemental Material at http://link.aps.org/supplemental/10.1103/PhysRevLett.117.045302 for the derivation of the effective Hamiltonian and its validity.
[37] A. Altland and M. R. Zirnbauer, Phys. Rev. B **55**, 1142 (1997).
[38] V. Gurarie, Phys. Rev. B **83**, 085426 (2011).
[39] J. Colpa, Physica (Amsterdam) **93A**, 327 (1978).
[40] V. Starzhinskii and V. Yakubovich, *Linear Differential Equations with Periodic Coefficients* (Wiley, London, 1975).
[41] J. Tomkovič, W. Muessel, H. Strobel, S. Löck, P. Schlagheck, R. Ketzmerick, and M. K. Oberthaler, arXiv:1509.01809.